High-spin Metal Centres in Dipolar EPR Spectroscopy

Originally published in:
Chimia 72(4), https://doi.org/10.2533/chimia.2018.216

Funding acknowledgement:
159707 - NMR studies in the Solid State (SNF)
146757 - NMR studies in the Solid State (SNF)
169057 - Generation of spin-label based restraints on biomolecular structure and their use in hybrid structure modelling (SNF)

doi:10.2533/chimia.2018.216 Chimia 72 (2018) 216–220

High-spin Metal Centres in Dipolar EPR Spectroscopy

Katharina Keller[§a], Thomas Wiegand[a], Riccardo Cadalbert[a], Beat H. Meier[a], Anja Böckmann[b], Gunnar Jeschke[a], and Maxim Yulikov*[a]

[§]SCS-Metrohm Award for best oral presentation in Physical Chemistry

Abstract: The substitution of Mg^{2+} by Mn^{2+} in the bacterial DnaB helicase from *Helicobacter pylori*, an ATP:Mg^{2+}-fuelled protein engine, allows electron paramagnetic resonance (EPR) spectroscopy to be performed on this system. EPR experiments make it possible to monitor nucleotide binding and to estimate the fraction of bound Mn^{2+} through relaxation measurements. Furthermore, by measuring spin–spin distances we probe the geometry within such multimeric assemblies using ultra-wideband double electron-electron resonance (DEER) and relaxation induced dipolar modulation enhancement (RIDME). The extraction of distance distributions from RIDME experiments on high-spin paramagnetic centres is influenced by the presence of dipolar frequency overtones. We show herein that we can correct for these overtones by using a modified kernel function in Tikhonov regularization analysis routines, and that the overtone coefficients for Mn^{2+} in the DnaB helicase are practically the same as in the previously studied Mn^{2+}–Mn^{2+} model compounds.

Keywords: Distance measurements · EPR spectroscopy · Gadolinium · Manganese · Motor proteins

Katharina Keller was born in Germany in 1989. In 2014 she obtained her Master's degree in Interdisciplinary Sciences from ETH Zürich with honours. She conducted her Master's thesis in the group of Prof. Christine Timmel at Oxford University, investigating lanthanide complexes by multi-frequency electron paramagnetic resonance (EPR). During her studies, she completed a research project at Neuroscience Research Australia in the field of magnetic resonance elastography. In Spring 2014, she was an intern at Philips Innovative Technologies working on magnetic resonance fingerprinting. Since 2015 she is a PhD student in the group of Prof. Gunnar Jeschke at ETH Zürich. Her work focuses on the investigation of metal centres suitable for dipolar EPR spectroscopy and the development of the relaxation-induced dipolar modulation enhancement technique, an emerging EPR pulse sequence for measuring spin–spin distances.

*Correspondence: Dr. M. Yulikov[a]
E-mail: maxim.yulikov@phys.chem.ethz.ch
[a]ETH Zurich
Laboratorium für Physikalische Chemie
Vladimir-Prelog-Weg 2, CH-8093 Zurich
[b]Molecular Microbiology and Structural Biochemistry, Labex Ecofect
UMR 5086 CNRS/Université de Lyon, Lyon, France

Introduction

Unpaired electrons are the basis of electron paramagnetic resonance (EPR) spectroscopy. Electron pairing is usually energetically favourable and thus only a small fraction of known chemical or biochemical compounds contains native paramagnetic centres or can be put in paramagnetic states to exhibit an intrinsic EPR signal. Examples are studies of chemical reactivity in transition metal catalysis,[1–3] electron transfer reactions,[4,5] metalloproteins[6–10] or defects in solid-state materials as in semiconductors[11] or polymers.[12–14] On the other hand, chemically stable paramagnetic species can be attached to sites of interest by so-called site-directed spin labelling (SDSL) under a wide range of conditions.[15–17] The magnetic moment for electrons is much larger than for nuclei, inducing a larger Boltzmann spin polarization. Thus, as compared to nuclear magnetic resonance (NMR), in EPR spectroscopy the detected photons have larger energies and stem from a larger fraction of unpaired spins at a given magnetic field and sample temperature. In favourable cases, in continuous wave experiments, EPR is able to detect about 10^{10} spins or concentrations down to 10 nM in aqueous solution, while the best pulse EPR spectrometers can detect spin concentrations down to the micromolar range and a total number of spins in the sub-nanomole range (~10^{12}–10^{13} spins). EPR studies can address the properties of electronic configuration for a single unpaired electron or a configuration of several unpaired electrons within one paramagnetic centre or cluster of a few strongly coupled spin centres. In this case, the information on the electronic configuration can be obtained by determining the parameters of the electron Zeeman (EZ) interaction, namely the g-tensor and the zero field splitting (ZFS) interaction. Electron–nuclear interactions are another source of information on the intrinsic electronic and geometric structure and on the local surrounding of the paramagnetic species. In this type of EPR investigations, the electron–nuclear hyperfine interactions, nuclear Zeeman and nuclear quadrupole interactions are analysed. As most of the above interactions are anisotropic, the detection of their time average, *e.g.* in solution, can also provide direct information about the dynamics of the paramagnetic centres under study.[9,18] In the presented work we describe yet another type of EPR experiment, where the weak magnetic dipole–dipole interactions in pairs of spin labels are detected to extract intramolecular distances in biomolecules.

At present, the most reliable way of extracting distances using EPR is the combination of SDSL utilizing nitroxide-based spin labels with the so-called Double Electron-Electron Resonance (DEER) experiment.[15–17,19–22] Nitroxides are well suited, as they are relatively small, sterically not demanding molecules with rather short linkers and the labelling chemistry is well established. Furthermore, nitroxides are sensitive to environmental parameters such as molecular motion on time scales between 10 ps and 1 ms, polarity, proticity, water or oxygen accessibility. Examples are the identification of secondary structure elements through nitroxide side chain mobility together with its solvent-accessibility or the detection of conformational changes in the range of µs-ms by time-resolved EPR.[15–17] Their EPR line shapes are relatively narrow, so that conventional microwave pulses can excite a sizeable fraction of all spins. It is important to keep in mind that several interactions usually exceed the excitation bandwidth of the strongest microwave pulses in EPR experiments and one often lacks the ability to excite the full spectrum, especially for metal centres.

Hence, why should we bother about using metal centres as spin probes, which typically exhibit much broader EPR spectra, are relatively large and bulky and are for the currently designed experiments less sensitive to their environment? There are several answers to this question. First, some metal centres are chemically more stable than nitroxides and thus EPR experiments can be performed under reducing conditions, *e.g.* in in-cell experiments.[23,24] Second, a valuable strategy in EPR, orthogonal spin-labelling, is based on using at least two different types of spins, which allows for spectroscopic selection of individual distances in multi-spin systems.[25–27] Third, intrinsically occurring metal centres in materials or metalloproteins as well as the possibility of substituting diamagnetic metal ions by paramagnetic ones motivate the development of EPR techniques. A highly interesting example for a wide variety of systems is the substitution of Mg^{2+} by Mn^{2+}, since ATP:Mg^{2+} binding and hydrolysis, as used in ATP-fuelled motors, is a very widespread mechanism in living systems. Here, we focus on the high-spin Kramers ions Gd^{3+} and Mn^{2+} with electron group spin and half-filled f and d shells, respectively. This results in a weak contribution of the orbital momentum to the total momentum causing a weak ZFS. The half-integer spin systems have a narrow central $|m = +1/2\rangle \leftrightarrow |m = -1/2\rangle$ transition and are very convenient for high-field/high-frequency applications, since this central transition narrows with increasing magnetic field strength.[27] Additionally, because the half-filled d or f shell leads to an isotropic *g*-value and isotropic metal hyperfine couplings, longitudinal and transverse magnetic relaxation of the metal ions Gd^{3+} and Mn^{2+} are slow compared to many other high-spin paramagnetic metal centres, so that pulse EPR experiments can be performed in glassy frozen solutions at temperatures up to at least 30 K. As a consequence of all these considerations, the choice of spin label depends on the problem at hand. In this contribution we want to give two examples using Mn^{2+} or Gd^{3+} as spin probes. In the first case, we will address advantages and disadvantages of using high spin Gd^{3+} ions in combination with the Relaxation Induced Dipolar Modulation Enhancement (RIDME) experiment for distance measurements. In the second case, we demonstrate what insights can be obtained by the substitution of diamagnetic Mg^{2+} by paramagnetic Mn^{2+} in a DnaB helicase using EPR spectroscopy.[28]

Gd^{3+}-based Distance Measurements

Site-to-site distance distributions, which can be computed from the dipolar spin–spin interaction, are an important type of structural information, for instance for biomolecules. To determine this interaction from EPR studies, it is necessary to observe a fraction of spins (A spins) while for another fraction of spins (B spins) their magnetization direction is inverted.[18,19] The inversion of B spins is achieved either by a microwave pulse at a second frequency, such as in the DEER experiment,[29] or it can be achieved due to spontaneous flips of the B spins due to longitudinal relaxation events, such as in the RIDME experiment.[30] The build-up of the dipolar modulation in the A spin – B spin model is illustrated in Fig. 1c. Inversion of the spin B causes the inversion of the local field it induces at the position of spin A, which causes a shift of the resonance frequency of the A spin. This change in local field is dependent on the inverse cube of the A–B distance. The time evolution of the A spin with changed frequency results in a phase gain of $\pm\,\omega_{dd}t$. Thus, depending on the inversion efficiency λ of the coupled B spin, a fraction of the electron spin echo signal will oscillate with the dipolar frequency ω_{dd}. This fraction λ is often called dipolar modulation depth.

Fig. 1b shows a typical echo-detected EPR spectrum of a Gd^{3+}-complex, which

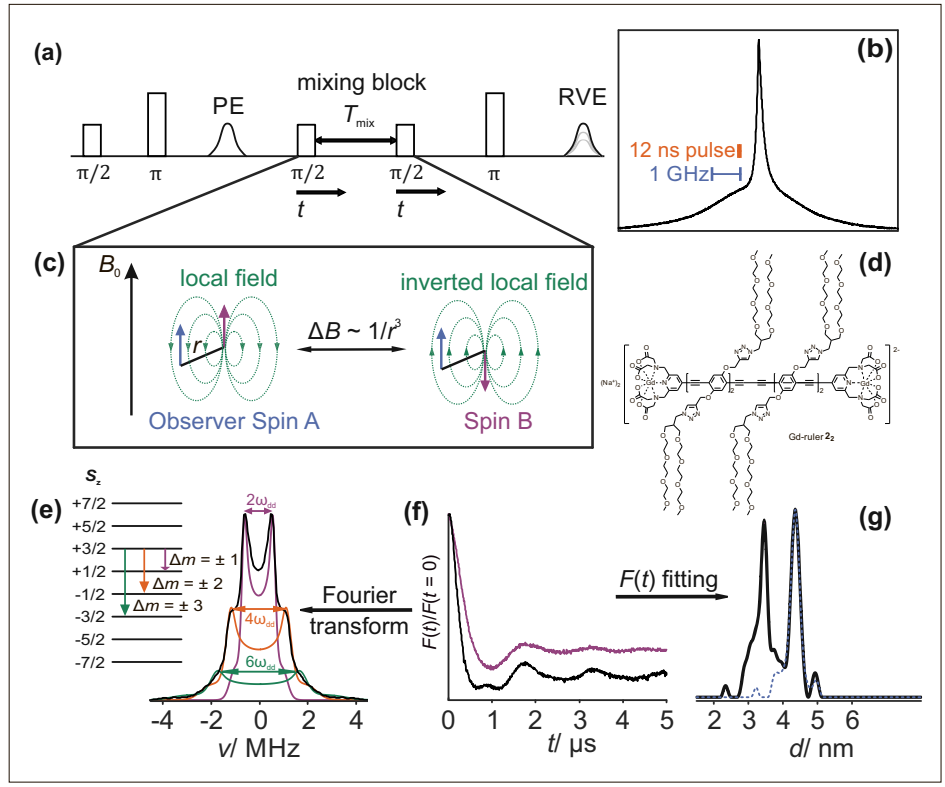

Fig. 1. (a) RIDME pulse sequence, (b) echo-detected EPR spectrum of the Gd^{3+} model compound, (c) schematic representation of the dipolar modulation build-up, (d) studied model compound (Gd-ruler 2_2), (e) frequency domain RIDME data with schematic representation of Gd^{3+}- energy levels neglecting ZFS and corresponding scaled Pake patterns for ω_{dd} (purple line), $2\omega_{dd}$ (orange line), $3\omega_{dd}$ (green line), (f) RIDME time-domain data (black line) and corresponding DEER data (purple line), (g) distance distribution resulting from Tikhonov regularization using the standard kernel (equation (2), black line) and a modified kernel function (Eqn. (3) with $P_2 = 0.4$ and $P_3 = 0.09$, dashed blue line).

spreads over a range of about 5 GHz. The orange bar indicates the bandwidth of a strong 12 ns pulse, which covers only a tiny fraction of the Gd^{3+}-spectrum. This means that we can only invert a small number of spins upon application of such pulses leading to a low modulation depth, which limits the reliability of extracted distance distributions. Over the last few years the methodology of broad-band chirp pulses has been transferred from NMR and optimized for use in EPR spectroscopy.[31–34] It was shown that modulation depths up to 20% could be achieved for Gd^{3+}–Gd^{3+} model compounds.[33] While it was shown that broad-band DEER can lead to a significant improvement, we found it tempting to also substitute the technically demanding broad-band spin inversion by a relaxation-based mechanism, which is utilized during the mixing block in the RIDME pulse sequence.[35]

The RIDME pulse sequence is shown in Fig. 1a.[35] The first two pulses generate electron spin coherence on the A spin, which refocuses to a primary echo (PE) and then defocuses again. The third pulse stores the observer magnetization along the direction of the external magnetic field in form of a polarization grating. The fourth pulse flips the magnetization back in the transverse plane where it is detected as a refocused virtual echo (RVE).[35] During the mixing block, spontaneous B spin flips occur and shift the resonance frequency of the A spin, which subsequently gains the phase $\pm \omega_{dd}t$. If the mixing block is stepped through with time t, the time evolution of the phase gain can be observed as a periodic oscillation with $\cos(\omega_{dd}t)$ on top of the intermolecular background decay.[30,35] A drawback of the RIDME technique is, however, the stronger background decay than in the DEER experiment, which results from a loss of RVE intensity by spectral diffusion during the mixing block. This loss is the stronger, the finer the polarization grating is and finesse of this grating increases with increasing time t between PE refocusing and storage of the magnetization by the first $\pi/2$ pulse. This non-exponential decay contribution makes the separation of the dipolar evolution function, the so-called intramolecular form factor $F(t)$, and the intermolecular background function more difficult and may complicate the measurement of long distances.[36] After removal of the background function, we need to invert Eqn. (1) to obtain the distance distribution $P(r)$[37–39]

$$F(t) = \int_0^\infty P(r)K(t,r)dr, \qquad (1)$$

where the kernel function $K(t,r)$ is

$$K(t,r) = \int_0^1 \cos[(3x^2-1)\omega_{dd}t]dx \quad (2)$$

This problem is ill-posed,[37] but can be stabilized by using Tikhonov regularization.[38–40] Given a fixed distance and spin flips with a change of electron spin magnetic quantum number of only $\Delta m_s = \pm 1$, the oscillation in the form factor can be parametrized with a single dipolar frequency ω_{dd} (Fig. 1f, purple curve). The Fourier transform of the form factor to frequency domain gives a scaled Pake pattern (Fig. 1e, purple curve). This pattern is characterized by two maxima, which are split by $2\omega_{dd}$, and has a total width of $4\omega_{dd}$. However, RIDME data,[36] obtained for a Gd-ruler compound[41] (Fig. 1d) exhibiting a narrow distance distribution with a mean distance of 4.3 nm,[33,42] show an oscillation pattern, which contains at least two further frequency contributions. Its Fourier transform exhibits additional shoulders, besides the two maxima (Fig. 1e, black curve). These shoulders can be attributed to Pake-like patterns of B spin transitions with $\Delta m_s = \pm 2$ (orange curve) and ± 3 (green curve) corresponding to the dipolar frequency overtones of $2\omega_{dd}$ and $3\omega_{dd}$.[43]

If the standard DEER data analysis routine[38] is applied to such high-spin RIDME data, an apparent multi-modal distance distribution results (Fig. 1g, black curve). The artefact peaks at $d_{exp}/\sqrt[3]{\Delta ms} = 3.0$ and 3.4 nm can be attributed to higher-order quantum transitions. In contrast, using a modified kernel function (Eqn. (3)) that accounts for the first two harmonic overtones, $2\omega_{dd}$ and $3\omega_{dd}$, with given weights P_2 and P_3, respectively, it was possible to accurately reconstruct the anticipated distance distribution (Fig. 1g, dashed blue curve).[36] The application of the RIDME pulse sequence resulted in traces with very high modulation depth of about up to 65% of the electron spin echo intensity.[36,43]

$$K_{mod}(r,t) = \int_0^1 \{P_1\cos[(3x^2-1)\omega_{dd}t] + P_2\cos[(3x^2-1)2\omega_{dd}t] + P_3\cos[(3x^2-1)3\omega_{dd}t]\}dx \qquad (3)$$

More details on the advantages and disadvantages of using ultra-wide band DEER and RIDME for high-spin centres can be found in previous publications.[33,34,36,43–46]

Paramagnetic Metal Ion Substitution of Mg^{2+} by Mn^{2+}

We now turn to the (double-) hexameric DnaB helicase from *Helicobacter pylori* *(Hp)* as an example for a biomolecule. The motor protein is associated with DNA replication and it is believed to move along the nucleic acid phosphodiester backbone separating the double-stranded nucleic acid strands. The nucleotide binding domains (NBDs) act as engines utilizing the energy derived from adenosine triphosphate (ATP) hydrolysis. Binding of ATP requires a divalent metal ion, typically Mg^{2+}, as cofactor.[47] During the functional ATP-hydrolysis cycle, the geometry of and distances between the metal binding sites can vary, and insight into the functioning of such ATP-fuelled proteins can be gained by characterizing the interactions between the metal, ATP and the NBDs. Continuous wave (CW) and pulsed EPR methods can be applied by mimicking the nucleotide-bound state through using poorly hydrolysable ATP analogues, *e.g.* AMP-PNP,[47,48] or other mimics of hydrolysis-intermediate states, and by substituting the cofactor Mg^{2+} by paramagnetic Mn^{2+}.

CW EPR and pulsed EPR relaxation measurements allow to follow the binding of the Mn^{2+}-ions to the NBDs. The CW EPR spectrum of Mn^{2+} is dominated by six sharp lines arising from the hyperfine coupling to the ^{55}Mn nucleus (I = 5/2) in a fast tumbling regime (see $MnCl_2$ EPR spectrum in Fig. 2a, highlighted in grey). Coordination of Mn^{2+} to AMP-PNP induces a pronounced change in the line shape that is related to a longer rotational correlation time of the larger complex with lower symmetry inducing an anisotropic broadening of the six hyperfine lines. The change in ZFS leads to additional spectral features. Addition of *HpDnaB* (1:12 Mn^{2+}:*HpDnaB* monomer ratio) causes a further change of the spectrum by even stronger prolongation of the rotational correlation time as well as by changes in the ZFS due to a different ligand field. The change in ZFS is also observed in the echo-detected EPR spectra of glassy frozen solutions (Fig. 2b) as the width of the outer envelope of the Mn^{2+} spectra scales with the strength of the ZFS.

Protein binding can be further quantified by relaxation measurements. The presence of several paramagnetic metal centres in the close vicinity of each other in the DnaB multimer, and the use of protonated protein and deuterated buffer lead to a strong difference in the transverse relaxation for the Mn^{2+} centres bound to NBDs as compared to Mn^{2+} coordinated to AMP-PNP in deuterated solution (Fig. 2c). The main contribution to this difference is spin diffusion of protons that are more abundant near the protein metal binding sites. This spin diffusion causes a stronger stochastic fluctuation of the local hyperfine field at the electron spin for bound Mn^{2+} ions compared to free ones. Assuming that not all Mn^{2+} ions are bound to the protein,

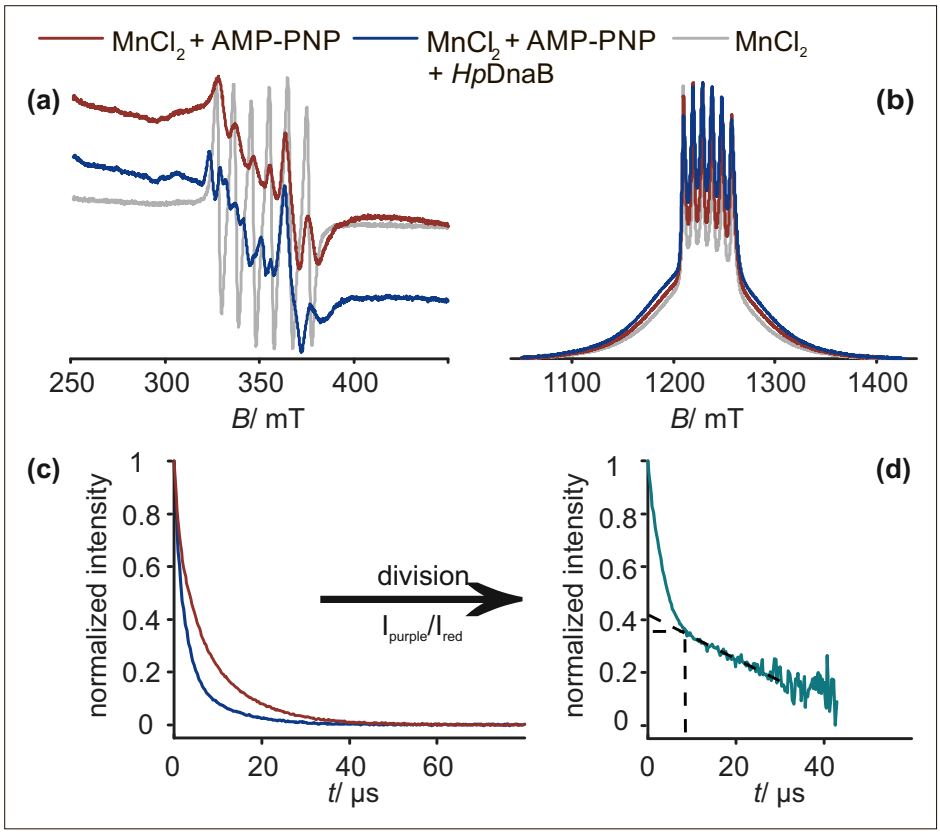

Fig. 2. (a) CW EPR, (b) echo-detected EPR spectra and (c) Hahn-echo decay curves of Mn^{2+} (from a $MnCl_2$ solution) (grey line), AMP-PNP:Mn^{2+} (red line) and DnaB:AMP-PNP:Mn^{2+} (blue line) (d) division trace from Hahn-echo decay curves. Adapted from ref. [28].

the electron spin echo decay would be a superposition of the contribution from protein-bound Mn^{2+} as well as solvent-exposed Mn^{2+}. Indeed, the transverse relaxation curve shows a fast initial decay, dominated by the bound species, and a slower decaying tail stemming from the unbound species. Using the Mn^{2+}:AMP-PNP echo decay as a reference for the slowly relaxing species, we can remove the contribution of the solvent-exposed Mn^{2+} by dividing the two time traces under the assumption that the relaxation pathway for the protein-bound species is independent of all other channels, and that the total relaxation rate is a sum of the rates of all relaxation pathways, *i.e.* relaxation processes are uncorrelated.[28,49,50] The division trace (Fig. 2d) reveals the fast component of the protein-bound relaxation pathway added to an approximately constant contribution resulting for the unbound relaxation pathway. That the contribution from unbound species is not constant may be related to additional intermolecular interactions as well as to correlation between relaxation processes. The crossing point rather accurately marks the relative fraction of bound to unbound species, which is in the presented case about 3 to 2.[28]

In this system, even for deuterated DnaB samples used to measure dipole–dipole interactions, the relaxation of Mn^{2+} ions bound to NBDs is faster than in the free state. For the case of incomplete binding, this leads to a very small modulation depth in the DEER experiment. The modulation depth is further reduced due to the broad EPR spectra of Mn^{2+} ions (Fig. 2b). Therefore, we conducted DEER experiments in Q band (34 GHz) using wideband pulses of a total bandwidth of 0.8–1.2 GHz. The resulting distance distribution obtained by Tikhonov regularization analysis[38] is shown in Fig. 3c. The distance peaks of 3 nm and, with lower significance, of 5–6 nm, are in rather good agreement with the (double-)hexameric assembly in *HpDnaB* from the homology model (inset in Fig. 3b) based on the structure of the *Aa*DnaB:ADP:Mg^{2+} complex obtained crystallographically.[51] Remaining flexibility or unspecifically bound Mn^{2+} may induce the less significant peaks in the range between 3.4 and 4 nm.

It is important to note that at least a full dipolar oscillation needs to be detected to extract the corresponding distances (see colour coding in Fig. 3c,f). Thus, distances larger than 7 nm are not accessible from the data presented.[28] Even with the use of wideband pump pulses only a low inversion efficiency of about 1.5% could be achieved (see Fig. 3b). Therefore, we investigated if the use of the RIDME sequence can improve the inversion efficiency. RIDME data were acquired in W band (94 GHz) due to the stronger appearance of electron spin echo envelope modulations in the RIDME experiment in Q band (34 GHz).[52–54] The resulting time trace is shown in Fig. 3d. After background correction, the depth of dipolar modulation amounts to about 6% considering that the first sharp initial decay is attributed to an artefact peak (Fig. 3e). The time trace is about four times shorter than the DEER time traces, since longer RIDME traces exhibited strong artefact peaks. Processing of the data with the standard routine, we observe two distinct peaks around 2.4 and 3 nm (Fig. 3f, black curve). This corresponds exactly to a primary frequency ω_{dd} of a 3 nm distance as well as its first overtone $2\omega_{dd}$. If the modified kernel function from Eqn. (3) and coefficients $P_2 = 0.5$ and $P_3 = 0.1$ obtained for Mn^{2+} ruler compounds[44] are used for data processing we obtain a relatively clean distance distribution in agreement with the DEER data presented above (Fig. 3f, cyan curve). Yet, for the currently available trace length, we cannot detect distances longer than 4 nm. It is promising that the RIDME overtone coefficients are similar for DnaB and for earlier published Mn^{2+}–Mn^{2+} model compounds.[44,55] However, more examples are required to ascertain that the calibrated overtone coefficients are generally applicable. Furthermore, it is necessary to reduce artefacts in RIDME. Complementary information on the conformational properties of the ATP:Mg^{2+}-binding site were obtained by solid-state NMR spectra, showing the high benefit of combining different techniques to obtain deeper insights in the systems under investigation.[28]

Conclusion

Application of EPR to metal centres in biological systems allows to monitor nucleotide binding, to estimate the fraction of bound Mn^{2+} through relaxation measurements, and to extract spin–spin distances to probe the geometry of multimeric assemblies using the ultra-wideband DEER as well as the RIDME technique. To widely employ the RIDME technique, the approach still needs to be improved. The reliability of background correction needs to be investigated and strategies to reduce artefact peaks in the distribution of dipole couplings need to be developed. For high-spin metal centres, validity of a set of constant overtone coefficients in the RIDME kernel should be tested on a larger set of systems. The combination of different EPR, NMR as well as other spectroscopic techniques provides more information on the system and improves reliability of this information. Such integrative approaches are thus valuable in structural biology.

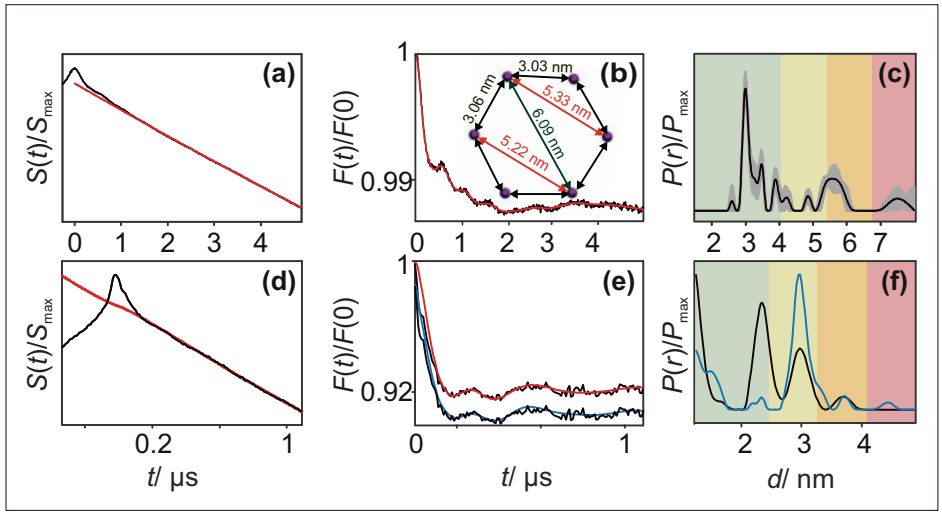

Fig. 3. Data obtained from (a)-(c) DEER, (d)-(f) RIDME measurements on a DnaB:AMP-PNP:Mn^{2+} system. (a), (d) primary data and background fit (red line), (b), (e) background-corrected form factors (black lines) and corresponding fit (coloured lines), (c), (f) resulting distance distributions. The color-coding indicates reliability ranges resulting from the limited length of the dipolar evolution trace. Pale green: Shape of distance distribution is reliable. Pale yellow: Mean distance and width are reliable. Pale orange: Mean distance is reliable. Pale red: Long-range distance contributions may be detectable, but cannot be quantified. (b) The inset shows the model obtained by homology. (e) Red: fit using the kernel from Eqn. (2), blue: fit using the kernel from Eqn. (3). (f) Black: using the kernel from Eqn. (2), blue: fit using the kernel from Eqn. (3) with $P_2 = 0.5$ and $P_3 = 0.1$, (c) the shaded areas give an error estimate of the distance distribution from a validation procedure. (b), (c) reproduced with permission of Wiley-VCH from ref. [28].

Acknowledgment

This work was supported by the Swiss National Science Foundation (Grant 200020_159707, 200020_146757 and 200020_169057), the French ANR (ANR-14-CE09-0024B) and the ETH Career SEED-69 16-1. The work of A.B. was performed within the framework of the LABEX ECOFECT (ANR-11-LABX-0048) of Université de Lyon, within the program 'Investissements d'Avenir' (ANR-11-IDEX-0007) operated by the French National Research Agency (ANR). We would like to thank Simon Widler for support with the sample preparation and Andrin Doll as well as Frauke Breitgoff for introduction to the AWG setup.

Received: January 24, 2018

[1] A. Bruckner, *Chem. Soc. Rev.* **2010**, *39*, 4673.
[2] S. Van Doorslaer, D. M. Murphy, in 'EPR Spectroscopy: Applications in Chemistry and Biology', Eds. M. Drescher, G. Jeschke, Springer Berlin Heidelberg, Berlin, Heidelberg, **2012**, pp. 1–39.
[3] E. Carter, D. M. Murphy, *Top. Catal.* **2015**, *58*, 759.
[4] D. M. Martino, H. van Willigen, M. T. Spitler, *J. Phys. Chem. B* **1997**, *101*, 8914.
[5] Z. E. X. Dance, Q. Mi, D. W. McCamant, M. J. Ahrens, M. A. Ratner, M. R. Wasielewski, *J. Phys. Chem. B* **2006**, *110*, 25163.
[6] R. Davydov, B. M. Hoffman, *P450 Catal. Mech.* **2011**, *507*, 36.
[7] W. Lubitz, E. Reijerse, M. van Gastel, *Chem. Rev.* **2007**, *107*, 4331.
[8] R. D. Britt, K. A. Campbell, J. M. Peloquin, M. L. Gilchrist, C. P. Aznar, M. M. Dicus, J. Robblee, J. Messinger, *Spec. Issue Dedic. Jerry Babcock* **2004**, *1655*, 158.
[9] S. Van Doorslaer, E. Vinck, *Phys. Chem. Chem. Phys.* **2007**, *9*, 4620.
[10] R. Cammack, in 'Spectroscopic Methods and Analyses: NMR, Mass Spectrometry, and Metalloprotein Techniques', Eds. C. Jones, B. Mulloy, A. H. Thomas, Humana Press, Totowa, NJ, **1993**, pp. 327–344.
[11] G. D. Watkins, *Phys. Solid State* **1999**, *41*, 746.
[12] G. Jeschke, *Macromol. Rapid Commun.* **2002**, *23*, 227.
[13] V. I. Krinichnyi, *J. Chem. Phys.* **2008**, *129*, 134510.
[14] D. Hinderberger, *Top. Curr. Chem.* **2012**, *321*, 67.
[15] J. P. Klare, H.-J. Steinhoff, *Photosynth. Res.* **2009**, *102*, 377.
[16] E. Bordignon, in 'EPR Spectroscopy: Applications in Chemistry and Biology', Eds. M. Drescher, G. Jeschke, Springer Berlin Heidelberg, Berlin, Heidelberg, **2012**, pp. 121–157.
[17] W. L. Hubbell, C. J. Lopez, C. Altenbach, Z. Yang, *Curr. Opin. Struct. Biol.* **2013**, *23*, 725.
[18] A. Schweiger, G. Jeschke, 'Principles of pulse electron paramagnetic resonance', Oxford University Press, **2001**.
[19] G. Jeschke, *Annu. Rev. Phys. Chem.* **2012**, *63*, 419.
[20] G. Jeschke, Y. Polyhach, *Phys. Chem. Chem. Phys.* **2007**, *9*, 1895.
[21] O. Schiemann, T. F. Prisner, *Q. Rev. Biophys.* **2007**, *40*, 1.
[22] G. E. Fanucci, D. S. Cafiso, *Curr. Opin. Struct. Biol.* **2006**, *16*, 644.
[23] M. Qi, A. Groß, G. Jeschke, A. Godt, M. Drescher, *J. Am. Chem. Soc.* **2014**, *136*, 15366.
[24] A. Martorana, G. Bellapadrona, A. Feintuch, E. Di Gregorio, S. Aime, D. Goldfarb, *J. Am. Chem. Soc.* **2014**, *136*, 13458.
[25] M. Yulikov, *Electron Paramagn. Reson.* **2015**, *24*, 1.
[26] E. Narr, A. Godt, G. Jeschke, *Angew. Chem. Int. Ed.* **2002**, *41*, 3907.
[27] D. Goldfarb, *Phys. Chem. Chem. Phys.* **2014**, *16*, 9685.
[28] T. Wiegand, D. Lacabanne, K. Keller, R. Cadalbert, L. Lecoq, M. Yulikov, L. Terradot, G. Jeschke, B. H. Meier, A. Böckmann, *Angew. Chem. Int. Ed.* **2017**, *56*, 3369.
[29] M. Pannier, S. Veit, A. Godt, G. Jeschke, H. Spiess, *J. Magn. Reson.* **2000**, *142*, 331.
[30] L. V. Kulik, S. A. Dzuba, I. A. Grigoryev, Y. D. Tsvetkov, *Chem. Phys. Lett.* **2001**, *343*, 315.
[31] A. Doll, S. Pribitzer, R. Tschaggelar, G. Jeschke, *J. Magn. Reson.* **2013**, *230*, 27.
[32] P. E. Spindler, S. J. Glaser, T. E. Skinner, T. F. Prisner, *Angew. Chem. Int. Ed.* **2013**, *52*, 3425.
[33] A. Doll, M. Qi, N. Wili, S. Pribitzer, A. Godt, G. Jeschke, *J. Magn. Reson.* **2015**, *259*, 153.
[34] A. Doll, M. Qi, S. Pribitzer, N. Wili, M. Yulikov, A. Godt, G. Jeschke, *Phys. Chem. Chem. Phys.* **2015**, *17*, 7334.
[35] S. Milikisyants, F. Scarpelli, M. G. Finiguerra, M. Ubbink, M. Huber, *J. Magn. Reson.* **2009**, *201*, 48.
[36] K. Keller, V. Mertens, M. Qi, A. I. Nalepa, A. Godt, A. Savitsky, G. Jeschke, M. Yulikov, *Phys. Chem. Chem. Phys.* **2017**, *19*, 17856.
[37] G. Jeschke, A. Koch, U. Jonas, A. Godt, *J. Magn. Reson.* **2002**, *155*, 72.
[38] G. Jeschke, V. Chechik, P. Ionita, A. Godt, H. Zimmermann, J. Banham, C. R. Timmel, D. Hilger, H. Jung, *Appl. Magn. Reson.* **2006**, *30*, 473, *http://www.epr.ethz.ch/software.html*.
[39] G. Jeschke, G. Panek, A. Godt, A. Bender, H. Paulsen, *Appl. Magn. Reson.* **2004**, *26*, 223.
[40] Y.-W. Chiang, P. P. Borbat, J. H. Freed, *J. Magn. Reson.* **2005**, *172*, 279.
[41] M. Qi, M. Hülsmann, A. Godt, *J. Org. Chem.* **2016**, *81*, 2549.
[42] A. Dalaloyan, M. Qi, S. Ruthstein, S. Vega, A. Godt, A. Feintuch, D. Goldfarb, *Phys. Chem. Chem. Phys.* **2015**, *17*, 18464.
[43] S. Razzaghi, M. Qi, A. I. Nalepa, A. Godt, G. Jeschke, A. Savitsky, M. Yulikov, *J. Phys. Chem. Lett.* **2014**, *5*, 3970.
[44] K. Keller, M. Zalibera, M. Qi, V. Koch, J. Wegner, H. Hintz, A. Godt, G. Jeschke, A. Savitsky, M. Yulikov, *Phys. Chem. Chem. Phys.* **2016**, *18*, 25120.
[45] A. Collauto, V. Frydman, M. D. Lee, E. H. Abdelkader, A. Feintuch, J. D. Swarbrick, B. Graham, G. Otting, D. Goldfarb, *Phys. Chem. Chem. Phys.* **2016**, *18*, 19037.
[46] A. Meyer, O. Schiemann, *J. Phys. Chem. A* **2016**, *120*, 3463.
[47] A. Bazin, M. V. Cherrier, I. Gutsche, J. Timmins, L. Terradot, *Nucleic Acids Res.* **2015**, *43*, 8564.
[48] T. Wiegand, R. Cadalbert, C. Gardiennet, J. Timmins, L. Terradot, A. Böckmann, B. H. Meier, *Angew. Chem. Int. Ed.* **2016**, *55*, 14164.
[49] S. Razzaghi, E. K. Brooks, E. Bordignon, W. L. Hubbell, M. Yulikov, G. Jeschke, *ChemBioChem* **2013**, *14*, 1883.
[50] P. Lueders, S. Razzaghi, H. Jäger, R. Tschaggelar, M. A. Hemminga, M. Yulikov, G. Jeschke, *Mol. Phys.* **2013**, *111*, 2824.
[51] M. S. Strycharska, E. Arias-Palomo, A. Y. Lyubimov, J. P. Erzberger, V. L. O'Shea, C. J. Bustamante, J. M. Berger, *Mol. Cell* **2013**, *52*, 844.
[52] A. V. Astashkin, in 'Methods in Enzymology', Eds. P. Z. Qin, K. Warncke, Academic Press, **2015**, vol. 563, pp. 251–284.
[53] D. Abdullin, F. Duthie, A. Meyer, E. S. Muller, G. Hagelueken, O. Schiemann, *J. Phys. Chem. B* **2015**, *119*, 13534.
[54] K. Keller, A. Doll, M. Qi, A. Godt, G. Jeschke, M. Yulikov, *J. Magn. Reson.* **2016**, *272*, 108.
[55] D. Akhmetzyanov, H. Y. V. Ching, V. Denysenkov, P. Demay-Drouhard, H. C. Bertrand, L. C. Tabares, C. Policar, T. F. Prisner, S. Un, *Phys. Chem. Chem. Phys.* **2016**, *18*, 30857.